

Effect of indium content on structural stability of Sn-inbinary alloys by first-principles calculation

J. J. Wang^a, X. Wang^b, X. M. Du^{b,*}, Y. Chi^c

^a*School of Science, Shenyang Ligong University, Shenyang 110159, China*

^b*School of Materials Science and Engineering, Shenyang Ligong University, Shenyang 110159, China*

^c*Party School of Liaoning Provincial Party Committee, Shenyang 110004, China*

Structural, electronic properties of the $\text{Sn}_x\text{In}_{(16-x)}$ ($x=7, 8, 9, 10, 12, 13, 14, 15$) solid solution alloys with tetragonal structure were investigated by means of first-principles calculations within the framework of density functional theory. The results of enthalpies of formation and cohesive energy show that the stability of the alloys increases with the decrease of the content In element. The electronic structure was further investigated to understand the underlying mechanism of the structural stability of the $\text{Sn}_x\text{In}_{(16-x)}$ alloys. $\text{Sn}_x\text{In}_{(16-x)}$ alloys exhibit a mixture characteristic of metallic and covalent bonding. A small quantity of In atoms in $\text{Sn}_x\text{In}_{(16-x)}$ alloys may improve significantly structural stability of alloys.

(Received July 27, 2021; Accepted October 22, 2021)

Keywords: $\text{Sn}_x\text{In}_{(16-x)}$ alloys, First-principles calculations, Phase stability, Electronicstructures

1. Introduction

In the field of microelectro-mechanical systems, the low-melting-point solders, such as pure indium (In), indium-tin (In-Sn) and indium-tin-bismuth (In-Sn-Bi) were applied in the fabrication and packaging of microoptical-electro-mechanical systems due to their excellent heat and electrical conductivity, such as Sn/In (melting point of 120 °C) and Sn/Bi (melting point of 138 °C)[1–3]. Many investigators have studied the phase equilibria of In-Sn [4,5] which are the constituent binary systems. The most promising In-Sn solders are based on the eutectic composition, In -48.3 at.% Sn which has been applied in the microoptical-electro-mechanical systems field with great potential for its long fatigue life and great ductility, compared with other solder alloys [6,7]. Koo and Jung et al. [6,7] studied the formation and growth of intermetallic compounds between In and Sn, such as the β phase (In_3Sn) and γ phase (InSn_4), which were characterized by tetragonal crystal and hexagonal structure, respectively. Shu Y.et al.[8] synthesized low melting temperature tin/indium (Sn/In) nanosolders with a wide In composition range (from 20 wt% to 70 wt%). by a surfactant-assisted chemical reduction method in an aqueous solution at ambient conditions. The lowest melting temperature was found to be 115.5 °C. Moreover, Witusiewicz et al. [9] precisely determine the solubility of the components in the coexisting phases at 77, 59 and 25 °C and to measure the enthalpies of melting of selected ternary alloys as to provide a more reliable description of the phase equilibria for the entire Bi-In-Sn system. Ramos et al.[10] determine the composition dependence of the structural and cohesive

* Corresponding author: du511@163.com

properties of $\text{Cu}_6(\text{Sn},\text{In})_5$ compounds using the projected augmented wave method, they found that composition dependence of the cohesive properties is the roughly linear dependence of the cohesive energy on the In content. However, studies on the composition dependence of the structural stability and electronic structure of Sn-In binary alloys are still rare experimentally and theoretically.

The present work focuses solely on the density function theory (DFT) based ab initio atomistic computational method to study structural stability of Sn-In alloys. This issue is addressed by evaluating and comparing the energy effects involved in progressive filling with In at crystallographic sites originally occupied by Sn. Moreover, the composition dependence of the electronic structure of the Sn-In alloys will be discussed.

2. Computational methods

The $2 \times 1 \times 1$ supercells of $\text{Sn}_x\text{In}_{(16-x)}$ ($x=7, 8, 9, 10, 12, 13, 14, 15$) solid solution alloys investigated in this study were constructed mainly based on the Sn-type structural models. The Sn has a T12 crystal structure with space group $I4/mmm$ (No.139) where the Sn atom is in 2a (0, 0, 0) Wyckoff site. The tetragonal $2 \times 1 \times 1$ supercell contains 16 atoms. The different lattice positions of 2a Wyckoff site in Sn supercell of $2 \times 1 \times 1$ are replaced by In atom. The series of $\text{Sn}_x\text{In}_{(16-x)}$ such as Sn_7In_9 , Sn_8In_8 , Sn_9In_7 , $\text{Sn}_{10}\text{In}_6$, $\text{Sn}_{12}\text{In}_4$, $\text{Sn}_{13}\text{In}_3$, $\text{Sn}_{14}\text{In}_2$, Sn_{15}In , were obtained, where the weight percentages of In were 55.4%, 49.1%, 42.9%, 36.7%, 24.4%, 18.2%, 12.1% and 6.06% respectively. Fig. 1 show the structural models of $\text{Sn}_x\text{In}_{(1-x)}$ alloys. According to the Sn-In phase diagram, Sn_7In_9 and Sn_8Bi_8 are hypereutectic alloys and the rest is hypoeutectic alloys.

All calculations were performed using DFT as implemented in the Quantum-ESPRESSO [11]. The ion–electron interaction was modeled by ultrasoft pseudopotentials [12]. Generalized gradient approximation (GGA) with the PBE exchange–correlation functional [13] was used. The kinetic energy cut-off value for plane-wave expansions was set as 380 eV for all the calculations. The larger values of the cut-off energy of atomic wave functions have been tested, such as 400 eV, 450 eV and 500 eV etc. Tests indicated that the total energies of the crystals have been not obviously decreased. The k -point meshes for Brillouin zone sampling were constructed using Monkhorst–Pack scheme [14] with $6 \times 3 \times 3$ grids for all structural models. Convergence with respect to the k -point sampling for the Brillouin zone integration was tested independently on the these alloys using regular meshes of increasing density. Tests indicate that the total energy converges to 1 meV/atom. The valence electronic configurations were taken to be $5s^25p^2$ for Sn, $5s^25p^1$ for In. For all structures the lattice parameters, the volume and the atom positions were allowed to relax simultaneously. The relaxations of cell geometry and atomic positions were carried out using a conjugate gradient algorithm until the Hellman–Feynman force on each of the unconstrained atoms was less than $0.01 \text{ eV}/\text{\AA}$. The self-consistent calculations were considered to be converged when the difference in the total energy of the crystal did not exceed 10^{-6} eV at consecutive steps. After the structures are optimized, the total energies are recalculated self-consistently with the tetrahedron method [15]. The latter technique was also used to calculate the electronic density of states (DOS).

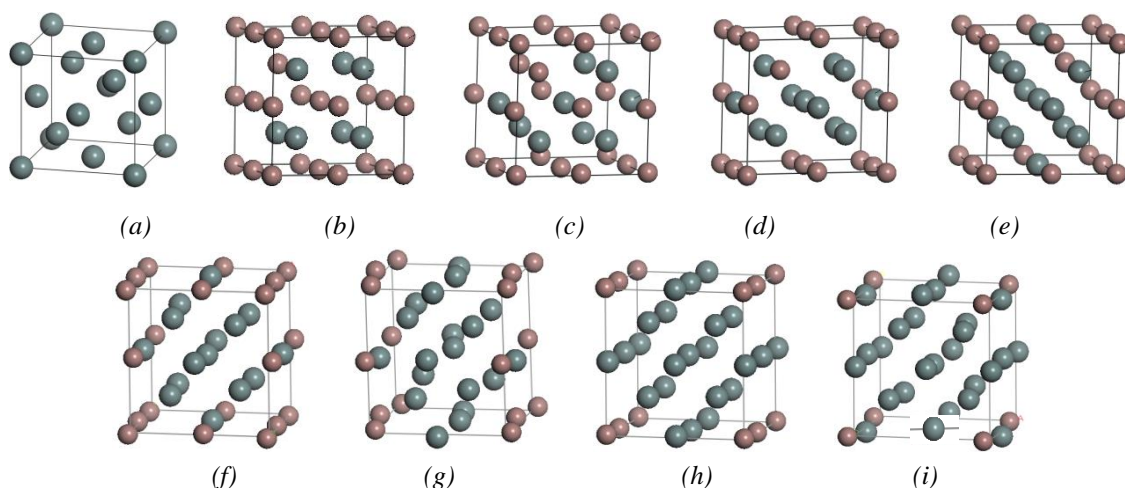


Fig. 1 Crystal structures of Sn and $\text{Sn}_x\text{In}_{(16-x)}$ alloys, (a) Sn, (b) Sn_7In_9 , (c) Sn_8In_8 , (d) Sn_9In_7 , (e) $\text{Sn}_{10}\text{In}_6$, (f) $\text{Sn}_{12}\text{In}_4$, (g) $\text{Sn}_{13}\text{In}_3$, (h) $\text{Sn}_{14}\text{In}_2$, (i) Sn_{15}In .

3. Results and discussion

3.1. Phase stability

Generally, the evaluation of the heat of formation per atom is relative to the composition-averaged energies of the pure elements in their equilibrium crystal structures [16]. The H_f of $\text{Sn}_x\text{In}_{(16-x)}$ structure at a low temperature can be expressed as follows:

$$H_f = (E_{\text{tot}} - N_{\text{Sn}}E_{\text{tot}}(\text{Sn})_{\text{solid}} - N_{\text{In}}E_{\text{tot}}(\text{In})_{\text{solid}}) / (N_{\text{Sn}} + N_{\text{In}}) \quad (1)$$

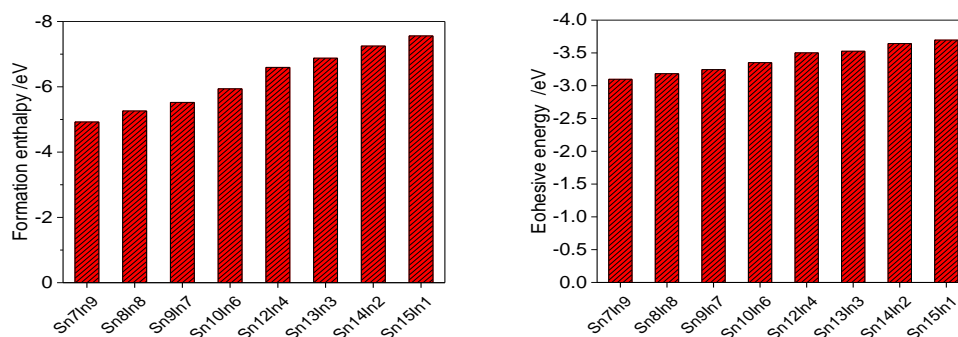
where E_{tot} is the total energy of $\text{Sn}_x\text{In}_{(16-x)}$ in equilibrium lattice per unit ; $E_{\text{tot}}(\text{Sn})_{\text{solid}}$ and $E_{\text{tot}}(\text{In})_{\text{solid}}$ are the total energy of tetragonal Sn and tetragonal In in their stable state per unit cell, respectively; N_{Sn} and N_{In} refer to the numbers of Sn and In atoms in unit cell of $\text{Sn}_x\text{In}_{(16-x)}$, respectively. In the present work, we calculate the single atomic energy by the following method: at first, the energy of a pure metal crystal in the solid state was calculated, then the energy was divided by the number of atoms involved in the crystal, and this result is the energy of a single atom in the pure metal. The calculated energies of Sn and In pure metals for our considered systems were -87.5691 eV and -1559.0614 eV, respectively. The calculated formation enthalpies of $\text{Sn}_x\text{In}_{(16-x)}$ alloys are shown in Fig. 2. Generally, the lower the formation enthalpy is, the more stable the crystal structure is. It was found that the formation enthalpies of $\text{Sn}_x\text{In}_{(16-x)}$ alloys decreased with the decrease of the content In atoms in structure model, indicating that the stability of the alloys increases correspondingly.

The cohesive energy (E_{coh}) can be expressed as follows:

$$E_{\text{coh}} = (E_{\text{tot}} - N_{\text{Sn}}E_{\text{tot}}(\text{Sn})_{\text{isolated}} - N_{\text{In}}E_{\text{tot}}(\text{In})_{\text{isolated}}) / (N_{\text{Sn}} + N_{\text{In}}) \quad (2)$$

where $E_{\text{tot}}(\text{Sn})_{\text{isolated}}$ and $E_{\text{tot}}(\text{In})_{\text{isolated}}$ are the total energy of the isolated constituent atoms at infinite separation.

In order to obtain an accurate value for the cohesive energy, the energy calculations for both isolated atom and the crystal must be performed at the same level of accuracy. The energy of an isolated atom has been calculated using a cubic supercell (irrespective of crystal structure of the corresponding solid) with large lattice parameter of 10\AA so that the inter atomic interaction is negligible. The calculated energies of isolated atoms Sn and In are -85.6870 and -1559.0967eV/atom , respectively. According to Eqs. (2), the obtained cohesive energies of $\text{Sn}_x\text{In}_{(16-x)}$ alloys are shown in Fig. 2. It is found that the cohesive energies of the $\text{Sn}_x\text{In}_{(16-x)}$ alloys decrease with the decrease of the content In atoms in structure models. In general, the cohesive intensity and structural stability of the crystal are correlated with its cohesive energy [17] being defined as either the energy needed to form the crystal from free atoms or the work needed to decompose the crystal into isolated atoms. The more negative cohesive energy is, the more stable is the corresponding crystal structure. The results have shown that the hypoeutectic Sn-In alloys is more stable than hypereutectic Sn-In alloys.



(a) Formation enthalpy H_f (b) Cohesive energy E_{coh}

Fig.2.Optimized results for $\text{Sn}_x\text{In}_{(16-x)}$ alloys.

3.2 Density of states

In order to investigate intrinsic mechanism for structural stability, the density of states (DOS) of $\text{Sn}_x\text{In}_{(16-x)}$ alloys were calculated. Fig. 2 shows the total densities of states (TDOS) and partial densities of states (PDOS) for $\text{Sn}_x\text{In}_{(16-x)}$ alloys, in which Fermi level was set to zero. It could be found that the hybridization of Sn-p and In-p, Sn-s and In-s, In-p and Sn-s states was believed to be the dominant factor for the stability improvement of $\text{Sn}_x\text{In}_{(16-x)}$ alloys. It can be seen from Fig.2 that the main bonding peaks of $\text{Sn}_x\text{In}_{(16-x)}$ alloys locate in the range from -11 eV to 3 eV, originating from the contribution of valance electron numbers of Sn-5s, Sn-5p, In-5s, In-5p. The bonding peaks appeared in the energy range from -11 eV to -5 eV, which were formed by the hybridization between the Sn-5s orbit and the In-5s orbit

. The bonding peaks appeared in the energy range from -5.0 eV to -3.0 eV were formed by the hybridization between the Sn-5p orbit and the In-5s orbit. For the bonding peaks in the energy range from -3.0 eV to 3.0 eV, the hybridization between the Sn-5p orbit and the In-5p orbit was predominant. As the content of In in $\text{Sn}_x\text{In}_{(16-x)}$ alloys decreased, the height of the bonding peaks between around -5eV and 3 eV decreased. It is indicated that the hybridization between the In-5s orbit and the Sn-5p orbit is continually weakening

. Moreover, the values of the total DOS at Fermi level are larger than zero for $\text{Sn}_x\text{In}_{(16-x)}$ alloys, which indicates the metallic behavior. The bonding electron numbers at the Fermi level, $N(E_F)$ for

Sn_7In_9 , Sn_8In_8 , Sn_9In_7 , $\text{Sn}_{10}\text{In}_6$, $\text{Sn}_{12}\text{In}_4$, $\text{Sn}_{13}\text{In}_3$, $\text{Sn}_{14}\text{In}_2$, $\text{Sn}_{15}\text{In}_1$ 8.82, 11.65, 9.52, 11.16, 8.26, 8.33, 8.25, 8.32, respectively. In general, $N(E_F)$ on DOS plot can be used to characterize the activity of valance electrons of the atoms in crystal. Namely, the smaller $N(E_F)$, the less is change probability of the electronic structures of the crystal when external conditions change, thus the crystal has the higher stability [18]. The stability of $\text{Sn}_x\text{In}_{(16-x)}$ alloys improved with the decrease of the content of In, which are entirely consistent with the results of the calculated enthalpies of formation cohesive energies.

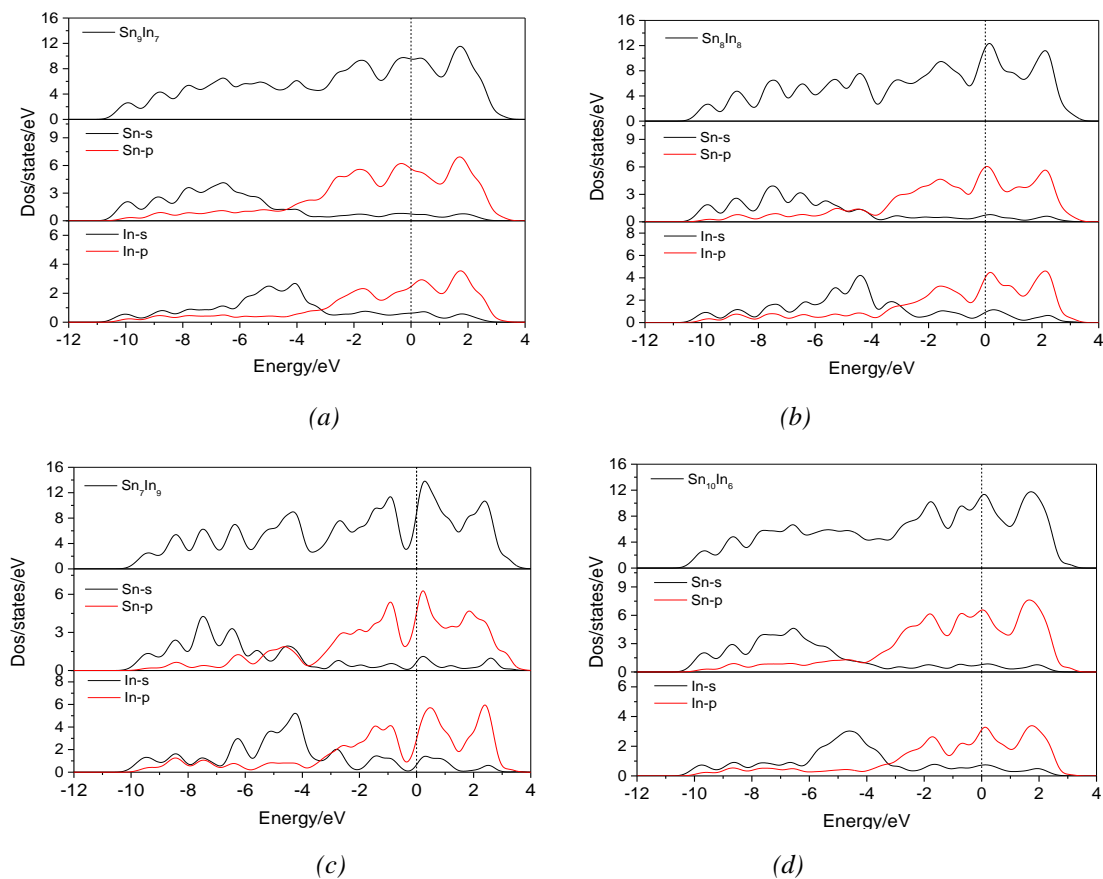


Fig. 3.1 .The calculated total density of states and partial densities of states of $\text{Sn}_x\text{In}_{(16-x)}$ alloys, (a) Sn_7In_9 , (b) Sn_8In_8 , (c) Sn_9In_7 ,

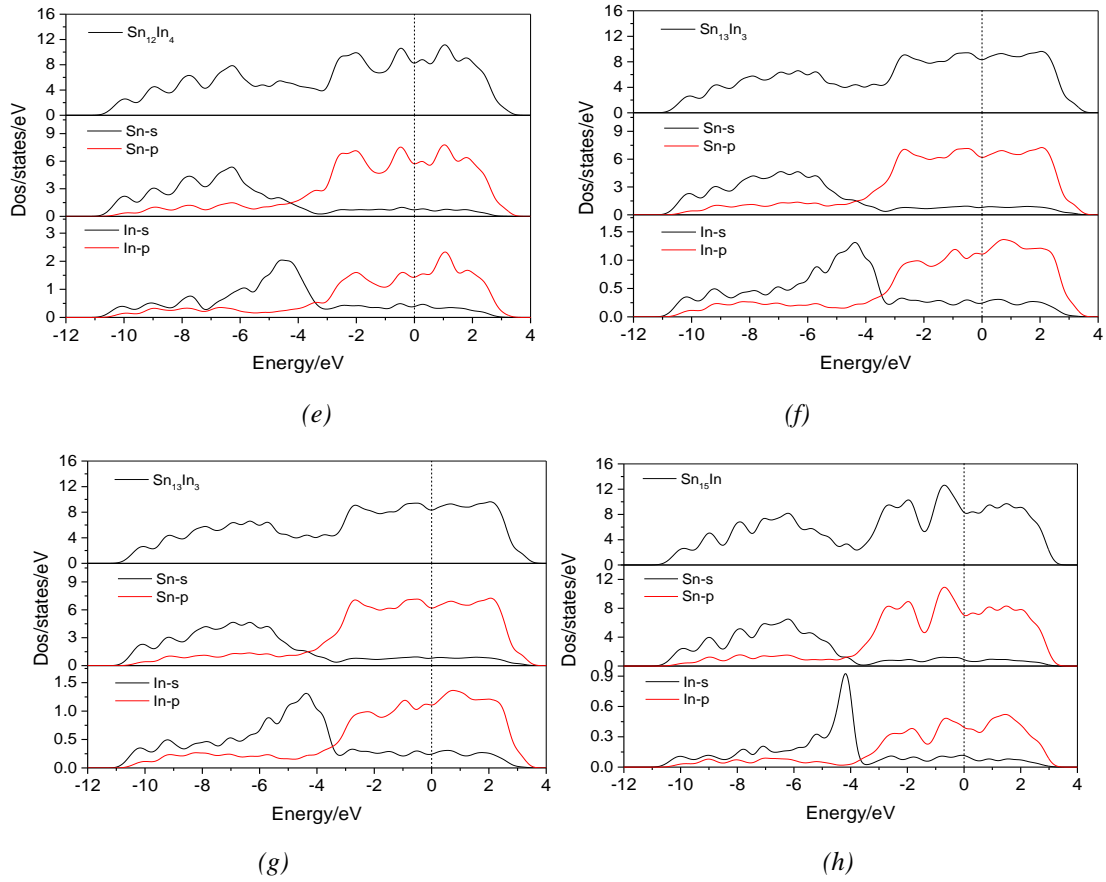


Fig. 3.2 The calculated total density of states and partial densities of states of $\text{Sn}_x\text{In}_{(16-x)}$ alloys, (e) $\text{Sn}_{12}\text{In}_4$, (f) $\text{Sn}_{13}\text{In}_3$, (g) $\text{Sn}_{14}\text{In}_2$, (h) Sn_{15}In .

3.3. Electron density difference

To visualize the nature of the bonding character and to explain the charge transfer and the bonding properties of $\text{Sn}_x\text{In}_{(16-x)}$ alloys, we investigated the redistribution of electron density due to In atom substitutions by electron density difference defined as

$$\Delta\rho(r) = \rho_{\text{cluster}}(r, \text{In}) - \rho_{\text{cluster}}(r) \quad (3)$$

where $\rho_{\text{cluster}}(r, \text{In})$ is the total electron density with In metal substitutions. Fig. 4 displays the calculated charge density difference distribution maps in the (110) plane for $\text{Sn}_x\text{In}_{(16-x)}$ alloys. In these figures, the In atoms and Sn atoms are in the center position. The color indicates charge transfer direction. The area of red stands for gaining electrons and the area of blue stands for losing the electrons. From Fig. 4, it can be seen that the non-spherical charge distribution around Sn and In atoms in all alloys which indicates that there are non-single metallic bonds. It is found that Sn atoms transfer electrons to In atoms, causing that In atoms gain electrons and Sn atoms lose the electrons, as shown in Fig. 4. Meanwhile, electrons enrichment and poor regions are formed for Sn-Sn, Sn-In and In-In atoms in the process of electron transfer. It means that the Sn-Sn is covalent bond, as well as In-In, Sn-In. Even though there are no obvious electron transfers between adjacent atoms In-In, a large number of electrons exist in the region between Sn atoms and In atoms, meaning that covalent character exists in In-In bond. For Sn-Sn atoms, the

overlap of bonding electron density between Sn and Sn atoms becomes stronger and stronger with decrease of the content of In atoms in $\text{Sn}_x\text{In}_{(16-x)}$ alloys, indicating a covalent bonding nature with the s-p hybridization in Sn-matrix solid solution alloys. While for In-In atoms, the overlap of bonding electron density becomes weaker and weaker with decrease of the content of In atoms in $\text{Sn}_x\text{In}_{(16-x)}$ alloys. From Fig. 4(a), it is clear that Sn atoms are surrounded by In atoms with non-spherical regions, implying that valence electrons from Sn atoms are transferred to the regions around In atoms, and the Sn-In interaction is apparently covalents-p, s-s and p-p hybridizations. However, there exists the overlap for the electron density between Sn and Sn, shown as in Fig.4(d-f). This indicates a covalent bonding between Sn and Sn. And Sn-In interactions are relatively stronger than that of Sn-Sn. Clearly the stronger covalent interactions between Sn atoms and In atom have weakened the interactions between In atom and In atom and between Sn atom and Sn atom. Therefore, a small quantity of In atoms in $\text{Sn}_x\text{In}_{(16-x)}$ alloys may improve significantly their mechanical properties. According to those analyses, $\text{Sn}_x\text{In}_{(16-x)}$ alloys exhibit a mixture characteristic of metallic and covalent bonding.

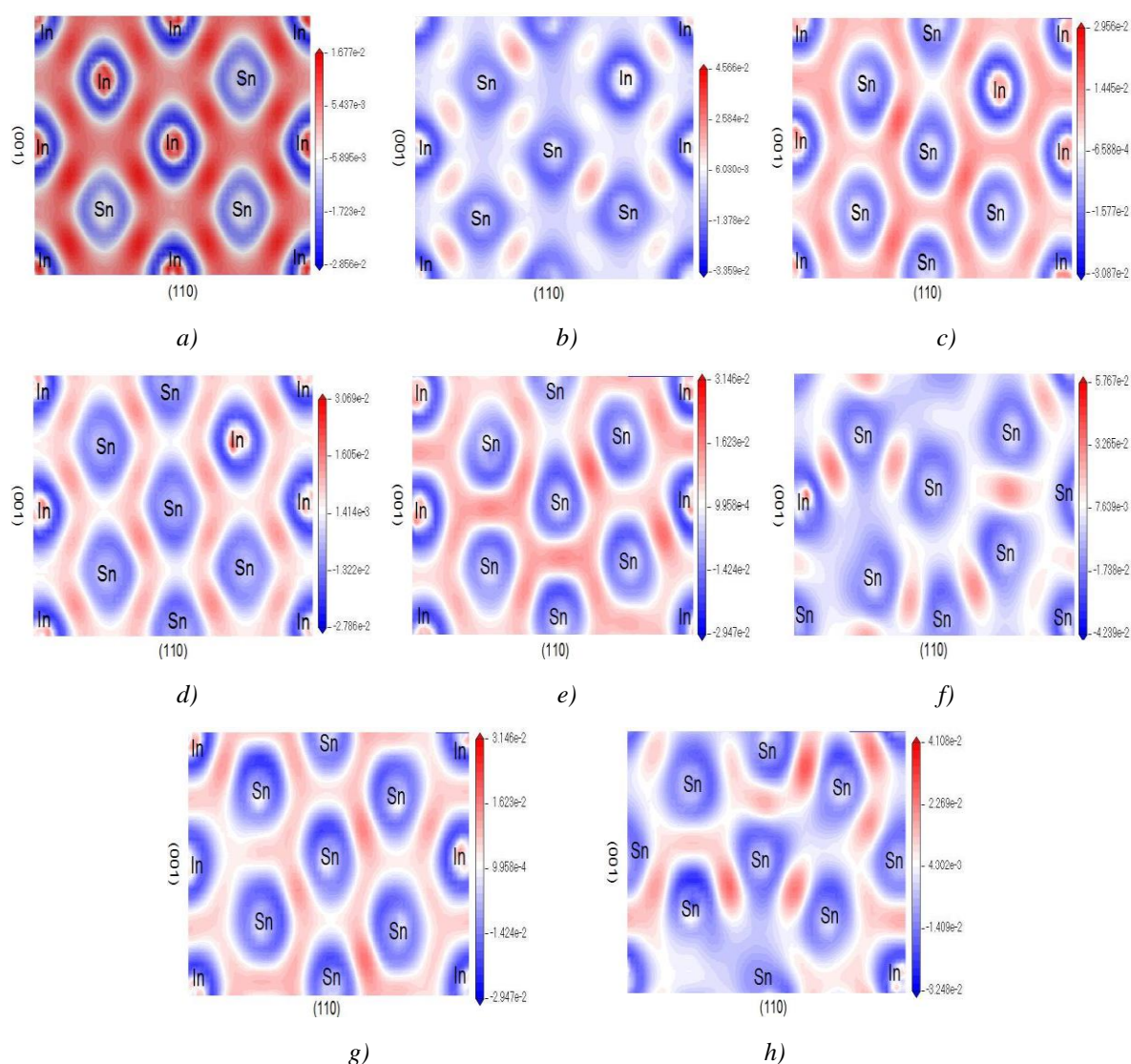


Fig. 4. The calculated electron density difference of $\text{Sn}_x\text{In}_{(16-x)}$ alloys, (a) Sn_7In_9 , (b) Sn_8In_8 , (c) Sn_9In_7 , (d) $\text{Sn}_{10}\text{In}_6$, (e) $\text{Sn}_{12}\text{In}_4$, (f) $\text{Sn}_{13}\text{In}_3$, (g) $\text{Sn}_{14}\text{In}_2$, (h) Sn_{15}In .

4. Conclusions

In conclusion, the investigation on the structural stability and electronic properties of $\text{Sn}_x\text{In}_{(16-x)}$ alloys has been performed by the plane-wave ultrasoft pseudopotential method based on the density-functional theory. The calculated enthalpies of formation and cohesive energy reveal that the stability of $\text{Sn}_x\text{In}_{(16-x)}$ alloys increases with the decrease of the content In. Electronic densities of states have shown that $\text{Sn}_x\text{In}_{(16-x)}$ alloys exhibit metallic characteristics and the s-p and p-p hybridizations in $\text{Sn}_x\text{In}_{(16-x)}$ alloys becomes continually weakening, as the content of In decreased. The electron density difference analysis demonstrates that owing to the electrons transfer from Sn to In, the (Sn-5s)–(Sn-5s) hybridization is less strong than the (Sn-5p)–(In-5p) and (Sn-5p)–(In-5s) hybridizations giving rise to a stronger stable effect for In than Sn.

Acknowledgements

This work was supported by Innovation talent Project of colleges and universities in Liaoning Province in 2020; Shenyang Young and Middle-aged Science and Technology Innovation Talents Project (RC180214 and RC200355) in Liaoning Province.

References

- [1] S.W. Chen, C.F. Yang, H.J. Wu, R.B. Chang, C.M. Hsu, *Mater. Chem. Phys.* **132**, 481 (2012).
- [2] X. Chen, F. Xue, J. Zhou, Y. Yao, *J. Alloys Compd.* **633**, 377 (2015).
- [3] J.W. Kim, S.B. Jung, *J. Nanosci. Nanotechnol.* **12**, 3259 (2012).
- [4] H. Okamoto, *Indium Alloys and Their Engineering Applications*, ed. C.E.T. White and H. Okamoto (Materials Park, OH: ASM Int.), 255 (1992).
- [5] B.J. Lee, C.S. Oh, J.H. Shim, *J. Electron. Mater.* **25**, 983 (1996).
- [6] J.M. Koo, S.B. Jung, *J. Electron. Mater.* **34**, 1565 (2005).
- [7] J.M. Koo, S.B. Jung, *Microsyst. Technol.* **13**, 1567 (2007).
- [8] Y. Shu, K. Rajathurai, F. Gao, Q. Z. Cui, Z. Y. Gu, *J. Alloys Compd.* **626**, 391 (2015).
- [9] V.T. Witusiewicz, U. Hecht, B. Bottger, S. Rex, *J. Alloys Compd.* **428**, 115 (2007).
- [10] S. B. Ramos, N. V. González Lemus, C. E. Deluque Toro, G. F. Cabeza, A. FernándezGuillermet, *J. Electron. Mater.* **46**, 4485 (2017).
- [11] <http://www.quantum-espresso.org/>
- [12] D. R. Hamann, M. Schluter, C. Chiang, *Phys. Rev. Lett.* **43**, 1494 (1979).
- [13] J. P. Perdew, K. Burke, M. Ernzerhof, *Phys. Rev. Lett.* **77**, 3865 (1996).
- [14] H. J. Monkhorst, J. D. Pack, *Phys. Rev. B* **13**, 5188 (1976).
- [15] P. E. Blochl, O. Jepsen, O. K. Andersen, *Phys. Rev. B* **49**, 16223 (1994).
- [16] G. Ghosh, M. Asta, *J. Mater. Res.* **20**, 3102 (2005).
- [17] V. I. Zubov, N. P. Tretiakov, J. N. Teixeira Rabelo, J. F. Sanchezortiz, *Phys. Lett. A* **198**, 470 (1995).
- [18] Y. Imai, M. Mukaida, T. Tsunoda, *Intermetallics* **8**, 381 (2000).